Front. Phys., 2011, 6(3): 251–257
DOI 10.1007/s11467-011-0180-5

RESEARCH ARTICLE

Optimal phase sensitivity of atomic Ramsey interferometers with coherent spin states

Guang-ri JIN[1,†], **Yong-chun LIU**[1,*], **Li YOU**[2]

[1] *Department of Physics, Beijing Jiaotong University, Beijing 100044, China*

[2] *Department of Physics, Tsinghua University, Beijing 100084, China*

[*] *Present address: State Key Lab for Mesoscopic Physics, School of Physics, Peking University, Beijing 100871, China*

E-mail: [†] *grjin@bjtu.edu.cn*

Received January 26, 2011; accepted February 25, 2011

We present a detailed analysis of phase sensitivity for a nonlinear Ramsey interferometer, which utilize effective mean-field interaction of a two-component Bose–Einstein condensate in phase accumulation. For large enough particle number N and small phase shift ϕ, analytical results of the Ramsey signal and the phase sensitivity are derived for a product coherent state $|\theta, 0\rangle$. When collisional dephasing is absent, we confirm that the optimal sensitivity scales as $2/N^{3/2}$ for polar angle of the initial state $\theta = \pi/4$ or $3\pi/4$. The best-sensitivity phase satisfies different transcendental equations, depending upon the initial state and the observable being measured after the phase accumulation. In the presence of the collisional dephasing, we show that the $N^{-3/2}$-scaling rule of the sensitivity maintains with spin operators $\hat{J}_x$ and $\hat{J}_y$ measurements. A slightly better sensitivity is attainable for optimal coherent state with $\theta = \pi/6$ or $5\pi/6$.

Keywords Ramsey interferometry, phase estimation, Bose–Einstein condensates, phase decay, one-axis twisting model

PACS numbers 03.75.Dg, 03.75.Mn, 03.75.Gg

1 Introduction

Phase estimation with its precision beyond shot-noise limit (SNL) is of significant importance for quantum interferometry and quantum metrology. In general, the achievable sensitivity depends on the input state [1–8], the observable being measured at output ports [9–11], and the coupling nature of the Hamiltonian in the phase accumulation [12–16]. It has been shown that a linear (Ramsey or Mach–Zehnder) interferometer with maximally entangled (N00N) state can achieve the Heisenberg limit [5–9], better than the SNL.

Nonlinear Ramsey interferometers with atomic Bose-Einstein condensates (BEC) have been discussed extensively [17–23]. In particular, a two-component condensate with the "one-axis twisting" Hamiltonian $\chi\hat{J}_z^2$ is a useful resource for generating spin squeezed states [24–28], as well as maximally entangled N00N states [29–32]. To efficiently control or manipulate the quantum states, it requires precise estimation of the mean-field interaction strength χ [33]. Utilizing the nonlinear interaction as phase shifter of the interferometer, the precision of χ can reach the Heisenberg limit even with a product coherent spin state (CSS) [13]. Perhaps more impressively, the so-called super-Heisenberg limit ($\propto 1/N^{3/2}$) can be obtained if an optimal CSS is injected into the phase shifter [14, 15]. Such a scaling is also achievable in nonlinear optical and nano-mechanical systems [12, 16].

For the BEC-based Ramsey interferometer, phase dephasing induced by atomic collisions and external field fluctuation gives rise to an enhanced decay of the Ramsey signal [34], which in turn degrades the achievable sensitivity. To what extend the dephasing will affect the achievable sensitivity is an important question. The role of the single-particle dephasing [35] on phase sensitivity of linear [36, 37] and nonlinear interferometers [13, 14] has been investigated previously. In a recent work [38], we further consider the influence of many-particle collisional dephasing on the BEC-based interferometer. Our analytical results confirm that the sensitivity of a small phase shift $\phi \sim 0$ can reach the super-Heisenberg limit with the $\hat{J}_y$ measurement [14].

Here, we present the details of Ref. [38] by focusing on the optimal sensitivity of the nonlinear interferometer with the collisional dephasing. For a small phase

shift and large particle number N, we derive analytical expressions of the Ramsey signals and the sensitivities for the initial coherent spin state $|\theta, 0\rangle$. Without the collisional dephasing, we find that the slop and the fluctuation of the Ramsey signal scale as $(N/2)^2$ and $\sqrt{N}/2$, respectively, which in turn leads to the super-Heisenberg-limited sensitivity for the optimal CSS with $\theta = \pi/4$ or $3\pi/4$ [14, 15]. In addition, the best-sensitivity phase with spin operator $\hat{J}_x$ measurement satisfies different transcendental equations and bifurcates at a critical value of the polar angle $\theta_{\rm cr}$. For a relatively large collisional dephasing, we prove analytically that the optimal CSS is changed to the case $\theta = \pi/6$ or $5\pi/6$ for both $\hat{J}_x$ and $\hat{J}_y$ measurements.

This paper is arranged as follows. In Section 2, we review quantum metrology protocols relying on the linear and the nonlinear interferometers. Solving the master equation, we obtain exact results of the signal and the variances for collective spin operators $\hat{J}_x$ and $\hat{J}_y$. In Section 3, we perform standard short-time analysis to the exact solutions and obtain analytical results of the phase sensitivities. Within the central few fringes, our results show a good agreement with numerical simulations. Scaling behaviors of the sensitivity are analyzed in Section 4 without and with the collisional dephasing. Finally, we conclude in Section 5 with the main results of our work.

2 Linear and nonlinear Ramsey interferometry

In most quantum metrology schemes, the system Hamiltonian can be described by ($\hbar = 1$):

$$\hat{H}_k = \Omega_x \hat{J}_x + \Omega_y \hat{J}_y + \chi(\hat{J}_z)^k \tag{1}$$

where the collective spin operators $\hat{J}_v = \sum_n \hat{\sigma}_v^{(n)}/2$, defined in terms of Pauli matrices $\hat{\sigma}_v$ with $v = x$, y, and z. The tunable Rabi frequencies $\Omega_x = {\rm Re}(\Omega)$ and $\Omega_y = {\rm Im}(\Omega)$ provide the Ramsey pulse or the beam splitter of the interferometers, and the last term with $k = 1$ or 2 contributes, respectively, to linear or nonlinear phase shifter.

In analogy with standard Ramsey (or Mach–Zehnder) interferometer, an input pulse is applied to the atoms with all spin up, yielding a coherent spin state [39, 40]: $|\theta, 0\rangle = {\rm e}^{-{\rm i}\theta\hat{J}_y}|J, J\rangle$, where the polar angle θ is given by the pulse area. Free evolution of the CSS for a duration t leads to the state vector $|\Psi_\theta(\phi)\rangle = {\rm e}^{-{\rm i}\phi(\hat{J}_z)^k}|\theta, 0\rangle$, with the phase shift $\phi = \chi t$, accumulated by the k-body Hamiltonian $\chi(\hat{J}_z)^k$ ($k = 1$ or 2). After the phase accumulation, an equatorial component of the collective spin $\hat{J}_x$ or $\hat{J}_y$ is measured to estimate the effective interaction strength χ [14]. Since the CSS prepared by the θ-pulse is Gaussian for large particle number N [25–27], the precision of the phase shift can be quantified by the error propagation formula:

$$\delta\phi_v = t\delta\chi_v = \frac{\Delta\hat{J}_v}{\left|{\rm d}\langle\hat{J}_v\rangle/{\rm d}\phi\right|}, \quad v = x \text{ or } y \tag{2}$$

where the Ramsey signal $\langle\hat{J}_v\rangle = \langle\Psi_\theta(\phi)|\hat{J}_v|\Psi_\theta(\phi)\rangle$ and the variance $\Delta\hat{J}_v \equiv (\langle\hat{J}_v^2\rangle - \langle\hat{J}_v\rangle^2)^{1/2}$ are evaluated with respect to the state vector $|\Psi_\theta(\phi)\rangle$. The observable $\hat{J}_x$ or $\hat{J}_y$ being measured after the phase accumulation is equivalent with a detection of population imbalance (i.e., the $\hat{J}_z$ measurement) to the output state: ${\rm e}^{-{\rm i}\frac{\pi}{2}\hat{J}_y}{\rm e}^{-{\rm i}\phi(\hat{J}_z)^k}{\rm e}^{-{\rm i}\theta\hat{J}_y}|J, J\rangle$ or ${\rm e}^{-{\rm i}\frac{\pi}{2}\hat{J}_x}{\rm e}^{-{\rm i}\phi(\hat{J}_z)^k}{\rm e}^{-{\rm i}\theta\hat{J}_y}|J, J\rangle$.

For the linear interferometer case (with $k = 1$), the achievable sensitivity is limited by the shot noise. To see it clearly, we calculate the signal and the variance of $\hat{J}_x$ as:

$$\begin{aligned} &\langle\hat{J}_x\rangle = J\sin\theta\cos\phi \\ &(\Delta\hat{J}_x)^2 = \frac{J}{2}(1 - \sin^2\theta\cos^2\phi) \end{aligned} \tag{3}$$

where $J = N/2$, $\phi = \chi t$, and θ is the polar angle of the initial CSS. Since the slop and the variance of the Ramsey signal ${\rm d}\langle\hat{J}_x\rangle/{\rm d}\phi \propto N/2$ and $\Delta\hat{J}_x \propto \sqrt{N}/2$, respectively, it is easy to find $\delta\phi_x = 1/\sqrt{N}$ (i.e., the SNL) for an optimal CSS with $\theta = \pi/2$ or $3\pi/2$. Replacing ϕ with $\phi + \pi/2$, we can obtain similar results for the $\hat{J}_y$ measurement.

In this paper, we focus on the nonlinear interferometer case. The Hamiltonian (1) with $k = 2$ describes an atomic Bose–Einstein condensate with two single-particle states [22, 23, 41]. In a real situation, collective spin excitation and external field fluctuations may lead to an enhanced phase diffusion of condensed atoms [25, 34]. To analyze it qualitatively, we assume that free evolution of the condensate system obeys the master equation [42–44]: ${\rm d}\hat{\rho}/{\rm d}t = {\rm i}[\hat{\rho}, \chi\hat{J}_z^2] + \mathcal{L}[\hat{\rho}]$, where the Liouvillian

$$\mathcal{L}[\hat{\rho}] = \Gamma(2\hat{J}_z\hat{\rho}\hat{J}_z - \hat{J}_z^2\hat{\rho} - \hat{\rho}\hat{J}_z^2) \tag{4}$$

with the dephasing rate Γ. For the single-particle case, Eq. (4) reduces to $\mathcal{L}[\hat{\rho}] = \Gamma(\hat{\sigma}_z\hat{\rho}\hat{\sigma}_z - \hat{\rho})/2$ [35], which has been investigated intensively for a linear [36, 37] and nonlinear interferometries [13, 14]. The many-body phase decoherence considered here, known as the collisional dephasing [42, 43], can be solved exactly with the density matrix elements $\rho_{m,n} \equiv \langle J, m|\hat{\rho}|J, n\rangle$ given by

$$\rho_{m,n}(\phi) = \rho_{m,n}(0){\rm e}^{{\rm i}(n^2-m^2)\phi - \gamma(m-n)^2\phi} \tag{5}$$

where the scaled dephasing rate $\gamma = \Gamma/\chi$ and $\rho_{m,n}(0) = c_m c_n^*$. For the initial CSS $|\theta, 0\rangle$, the probability amplitudes $c_m = \binom{2J}{J-m}^{1/2}\cos^{J+m}(\theta/2)\sin^{J-m}(\theta/2)$. Recently, the role of the phase diffusion on optical phase estimation has been investigated for continuous variable

Gaussian states and similar result of Eq. (5) has been obtained by Genoni *et al.* [45].

The expectation value of an operator $\hat{A}$ now becomes $\langle\hat{A}\rangle = \mathrm{Tr}(\hat{\rho}\hat{A})$. Using Eq. (5), it is easy to obtain $\langle\hat{J}_+\rangle = \mathrm{e}^{-\gamma\phi}\langle\hat{J}_+\rangle_0$ and $\langle\hat{J}_+^2\rangle = \mathrm{e}^{-4\gamma\phi}\langle\hat{J}_+^2\rangle_0$. Here, the subscript "0" denotes the expectation values in the absence of the dephasing (i.e., $\gamma = 0$). Previously, exact solutions of $\langle\hat{J}_+\rangle_0$ and $\langle\hat{J}_+^2\rangle_0$ have been obtained for arbitrary CSS [14, 26], which yield

$$\langle\hat{J}_+\rangle = J\sin\theta\mathrm{e}^{-\gamma\phi}\left[R(\phi)\right]^{2J-1} \tag{6}$$

$$\langle\hat{J}_+^2\rangle = J\left(J-1/2\right)\sin^2\theta\mathrm{e}^{-4\gamma\phi}\left[R(2\phi)\right]^{2J-2} \tag{7}$$

where

$$\begin{aligned} R(\phi) &= \cos\phi + \mathrm{i}\cos\theta\sin\phi \\ &= \left(1-\sin^2\theta\sin^2\phi\right)^{1/2}\mathrm{e}^{\mathrm{i}\cos\theta\tan\phi} \end{aligned} \tag{8}$$

Moreover, we obtain $\langle\hat{J}_z\rangle = J\cos\theta$ and $\langle\hat{J}_z^2\rangle = J^2 - J(J-1/2)\sin^2\theta$. Note that the collisional dephasing imposes an exponential decay to the phase coherence ($\propto\langle\hat{J}_+\rangle$), but keeps the population imbalance ($\propto\langle\hat{J}_z\rangle$) intact, as demonstrated recently by Widera *et al.* [34].

The numerator of Eq. (2) can be solved as $(\Delta\hat{J}_{x/y})^2 = \frac{1}{2}[J(J+1) - \langle\hat{J}_z^2\rangle \pm \mathrm{Re}\langle\hat{J}_+^2\rangle] - \langle\hat{J}_{x/y}\rangle^2$, where $\langle\hat{J}_x\rangle = \mathrm{Re}\langle\hat{J}_+\rangle$ and $\langle\hat{J}_y\rangle = \mathrm{Im}\langle\hat{J}_+\rangle$. The denominator of Eq. (2) requires special attention as $\mathrm{d}\langle\hat{J}_v\rangle/\mathrm{d}\phi = t^{-1}\mathrm{d}\langle\hat{J}_v\rangle/\mathrm{d}\chi$ for $v = x$ or y, where the derivative does not work at the exponential term of Eq. (6) since $\mathrm{e}^{-\gamma\phi} = \mathrm{e}^{-\Gamma t}$. Therefore, the slope for the Ramsey signal $\mathrm{d}\langle\hat{J}_x\rangle/\mathrm{d}\phi$ or $\mathrm{d}\langle\hat{J}_y\rangle/\mathrm{d}\phi$ is given by the real or imaginary part of $\mathrm{d}\langle\hat{J}_+\rangle/\mathrm{d}\phi$, with

$$\begin{aligned} \frac{\mathrm{d}\langle\hat{J}_+\rangle}{\mathrm{d}\phi} &= \mathrm{i}J(2J-1)\sin\theta\mathrm{e}^{-\gamma\phi}\left[R(\phi)\right]^{2J-2} \\ &\quad\times\ (\cos\theta\cos\phi + \mathrm{i}\sin\phi) \end{aligned} \tag{9}$$

In Fig. 1, exact numerical results of the sensitivity are plotted for the initial CSS with $\theta = \pi/4$ (*empty circles*) and $\pi/6$ (*solid red lines*). It is found that both $\delta\phi_x$ and $\delta\phi_y$ oscillate rapidly with the phase shift ϕ. Minimal value of the phase uncertainty, i.e., the best sensitivity, occurs for small enough phase shift $\phi < \pi/(\sqrt{2}J)$ (left panel of Fig. 1) or $\phi < 0.5\pi/(\sqrt{2}J)$ (right panel). In the following, we focus on the small-phase region and study the dependence of the best sensitivity with the polar angle θ. The case $\theta = 0$ or π will be excluded due to $\mathrm{d}\langle\hat{J}_v\rangle/\mathrm{d}\phi = 0$ and hence $\delta\phi_v \to \infty$ (with $v = x$, y), which implies that no information about χ can be gained for the input states with $\theta = 0$ and π.

3 Analytical results of the phase sensitivity

To investigate scaling behaviors of the sensitivities $\delta\phi_x$ and $\delta\phi_y$, we perform standard short-time analysis to the above exact results [24, 26]. In the limit $|\phi| = |\chi t| \ll 1$,

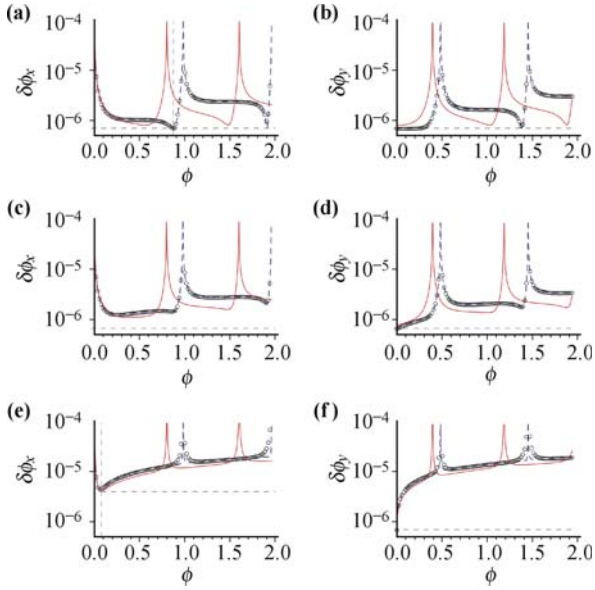

Fig. 1 Phase sensitivities $\delta\phi_x$ (*left*) and $\delta\phi_y$ (*right*) as a function of phase shift ϕ [in units of $\pi/(\sqrt{2}J)$] for $J = N/2 = 10^4$, $\gamma = 0$ (*top*), 1 (*middle*), and 10^2 (*bottom*), and $\theta = \pi/4$ (*empty circles*), $\pi/6$ (*solid red lines*). The dashed blue lines are analytical results for $\theta = \pi/4$, obtained from Eq. (16) and Eq. (17). Horizontal lines in **(a)**, **(b)**, **(c)**, **(d)**, and **(f)** denote the super-Heisenberg limit $1/(\sqrt{2}J^{3/2})$; while in **(e)** the horizontal line is $(2\gamma)^{1/3}/(\sqrt{2}J^{3/2})$. Vertical lines in (a) and (e) denote the best-sensitivity phase $\phi_{\min} = 0.89\times\pi/(\sqrt{2}J)$ and $(2\gamma)^{-1/3}/J$, respectively.

Eq. (8) can be approximated as

$$R(\phi) \simeq \mathrm{e}^{-\frac{1}{2}\phi^2\sin^2\theta}\mathrm{e}^{\mathrm{i}\phi\cos\theta} \tag{10}$$

so we have

$$\begin{aligned} \langle\hat{J}_+\rangle &\simeq J\sin\theta\mathrm{e}^{-\beta}\mathrm{e}^{\mathrm{i}(\alpha+\phi\cos\theta)} \\ \langle\hat{J}_+^2\rangle &\simeq J(J-1/2)\sin^2\theta\mathrm{e}^{-4\beta}\mathrm{e}^{2\mathrm{i}\alpha} \end{aligned} \tag{11}$$

where

$$\alpha = 2J\phi\cos\theta, \quad \beta = J\phi^2\sin^2\theta + \gamma\phi \tag{12}$$

For large enough J ($= N/2 \gg 1$), the phases of $\langle\hat{J}_+^2\rangle^{1/2}$ and $\langle\hat{J}_+\rangle$ are given by $\Phi_2 \simeq 2(J-1)\phi\cos\theta \simeq \alpha$ and $\Phi_1 \simeq (2J-1)\phi\cos\theta \simeq \alpha + \phi\cos\theta$, respectively. The phase difference $\Phi_1 - \Phi_2 \simeq \phi\cos\theta$ cannot be omitted since the best sensitivity occurs at $J\phi \sim 1$ in some situation [see for instance Fig. 1(a)]. Using the above approximated results, we obtain the variance

$$(\Delta\hat{J}_x)^2 \simeq \frac{J}{2}\left[1-(\eta_0 - J\eta_1)\sin^2\theta\right] \tag{13}$$

where $\eta_0 = [1+\mathrm{e}^{-4\beta}\cos(2\alpha)]/2$ and

$$\eta_1 = (1-\mathrm{e}^{-2\beta})[1-\mathrm{e}^{-2\beta}\cos(2\alpha)] + 2\phi\cos\theta\mathrm{e}^{-2\beta}\sin(2\alpha) \tag{14}$$

Substituting $\alpha \to \alpha + \pi/2$, one can also obtain similar expression of the variance $(\Delta\hat{J}_y)^2$. In addition, Eq. (9) can be approximated as

$$\frac{\mathrm{d}\langle\hat{J}_+\rangle}{\mathrm{d}\phi} \simeq 2\mathrm{i}J^2\sin\theta(\cos\theta+\mathrm{i}\phi)\mathrm{e}^{-\beta}\mathrm{e}^{\mathrm{i}\alpha} \tag{15}$$

For θ far away from $\pi/2$, it becomes $\mathrm{d}\langle\hat{J}_+\rangle/\mathrm{d}\phi \simeq \mathrm{i}J^2\sin(2\theta)\mathrm{e}^{\mathrm{i}\alpha}$, where we assume $J(J-1/2)\simeq J^2$ for large enough J and $\mathrm{e}^{-\beta}\simeq 1$.

From the above results, it is still hard to analyze scaling behaviors of the sensitivities. In order to get a closed form of the sensitivities, we now expand η_0 and η_1 up to the zeroth and the first-order of β, yielding $\eta_0\simeq\cos^2\alpha$, $\eta_1\simeq 4(\beta\sin\alpha+\phi\cos\theta\cos\alpha)\sin\alpha$. Inserting them into Eq. (13), we obtain the analytical expression of the sensitivity [38]:

$$(\delta\phi_x)^2 \simeq \frac{1+(\cos\theta\cot\alpha+2J\phi\sin^2\theta)^2+4\gamma J\phi\sin^2\theta}{2J^3\sin^2(2\theta)} \tag{16}$$

where we used $\mathrm{d}\langle\hat{J}_x\rangle/\mathrm{d}\phi\simeq -J^2\sin(2\theta)\sin\alpha$ for $\theta\neq\pi/2$. It is important to note that the slop of the Ramsey signal now oscillates with the amplitude $\propto(N/2)^2$, which is N times larger than the linear case [see Eq. (3)]. On the other hand, from Eq. (13) we find the variance $\Delta\hat{J}_x\propto\sqrt{N}/2$. As a result, the achievable sensitivity can reach the super-Heisenberg limit, i.e., $\delta\phi_x\sim 2/N^{3/2}$.

Replacing α with $\alpha+\pi/2$, we further obtain the phase sensitivity for the $\hat{J}_y$ measurement [38]:

$$(\delta\phi_y)^2 \simeq \frac{1+(\cos\theta\tan\alpha-2J\phi\sin^2\theta)^2+4\gamma J\phi\sin^2\theta}{2J^3\sin^2(2\theta)} \tag{17}$$

As shown in Fig. 1, our analytical results (*dashed blue lines*) show a good agreement with exact numerical simulations (*empty circles*) for the case $\theta=\pi/4$. Both $\delta\phi_x$ and $\delta\phi_y$ oscillate in a fringe pattern and diverge at the fringe boundaries $|\phi|=s\pi/(2J\cos\theta)$ and $(s+\frac{1}{2})\pi/(2J\cos\theta)$ for an integer $s=0,1,\cdots$, which are given respectively, by $\cot\alpha\to\infty$ in Eq. (16) and $\tan\alpha\to\infty$ in Eq. (17).

4 Scaling rules of the optimal sensitivity

In the previous sections, we provide the detailed derivations of Eq. (16) and Eq. (17), which shows a good agreement with the exact numerical simulations for small phase shift ϕ and large enough particle number N ($=2J>10^2$). Moreover, both of them are valid for the dephasing rate $\gamma<J^{3/4}$ and the initial CSS with $\theta\neq\pi/2$ (see below). We now analyze scaling rules of the best sensitivities.

4.1 Without the dephasing

First, let us consider the simplest case with $\gamma=0$. Via minimizing Eq. (16) with respect to ϕ, we find that local minima of $\delta\phi_x$ occur when the following transcendental equations are satisfied

$$\cos\theta\cot\alpha+2J\phi\sin^2\theta=0 \tag{18}$$

or

$$\sin\alpha=\cot\theta \tag{19}$$

Substituting Eq. (18) into Eq. (16), it is easy to obtain the best sensitivity [14]:

$$(\delta\phi_x)_{\min}\simeq\frac{1}{\sqrt{2}J^{3/2}\,|\sin(2\theta)|} \tag{20}$$

which depends on the number of atoms N ($=2J$) and the polar angle of the initial state θ. The super-Heinsenberg-limited sensitivity $(\delta\phi_x)_{\min}\simeq 1/(\sqrt{2}J^{3/2})=2/N^{2/3}$ is attainable for the CSS with $\theta=\pi/4$ or $3\pi/4$ [14]. In addition, Eq. (18) reduces to $\cot(\alpha)+\alpha=0$, which yields $\alpha=\sqrt{2}J\phi\simeq\pm 0.89\pi,\pm 1.95\pi$, etc. Hereafter, we focus on the first root and adopt the notation $\phi_{\min}=|\chi|_{\min}t$ to denote the best-sensitivity phase for a measurement of spin operator $\hat{J}_x$ or $\hat{J}_y$.

For the $\hat{J}_x$ measurement, the best sensitivity occurs at $\phi_{\min}\simeq 0.89\pi/(\sqrt{2}J)$ if the optimal input state with $\theta=\pi/4$ or $3\pi/4$ is adopted. The dependence of $\phi_{\min}$ on the θ is rather complicated [see empty circles of Fig. 2(a)]. A more careful investigation reveals the existence of a critical polar angle

$$\theta_{\mathrm{cr}}\simeq\arctan(0.6J^{1/8}) \tag{21}$$

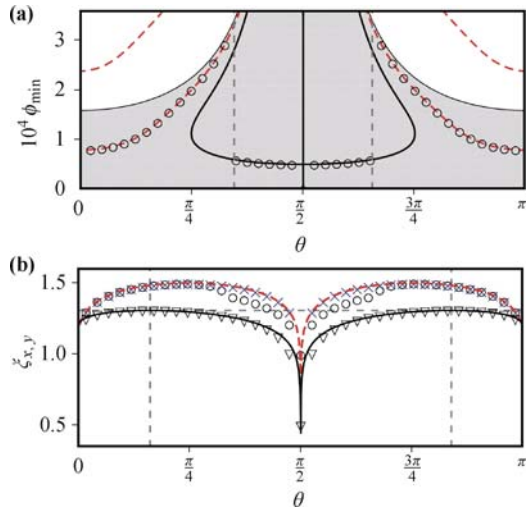

Fig. 2 **(a)** Numerical results of the best-sensitivity phase $\phi_{\min}$ with a $\hat{J}_x$ measurement (*empty circles*) as a function of the polar angle θ for $J=10^4$ and $\gamma=0$. The red dashed and solid lines denote, respectively, contour plots of Eqs. (18) and (19) within the central (*shaded*) fringe region $0\leqslant\phi_{\min}<\pi/(2J\cos\theta)$. **(b)** The scaling exponents ξ_x (*empty circles*) and ξ_y (*crosses*) for the case $J=10^4$ and $\gamma=0$, in a comparison to the analytical result of Eq. (23) (*red dashed*). Numerical results of ξ_x for $\gamma=10^2$ (*triangles*) fit well with Eq. (26) (*solid line*). The vertical grid lines in (a) and (b) denote the critical polar angle $\theta=\theta_{\mathrm{cr}}\simeq 1.383\times\pi/4$ and $\pi/6$ (also $\pi-\theta$), respectively, while the horizontal line in (b) denotes $3/2-\ln(2\gamma)/(3\ln J)$ with $\gamma=10^2$ and $J=10^4$.

which depends weakly on J, as shown in Fig. 3. For $\theta_{\rm cr} < \theta < (\pi - \theta_{\rm cr})$, the best-sensitivity phase $\phi_{\rm min}$ is in fact determined by Eq. (19), rather than Eq. (18).

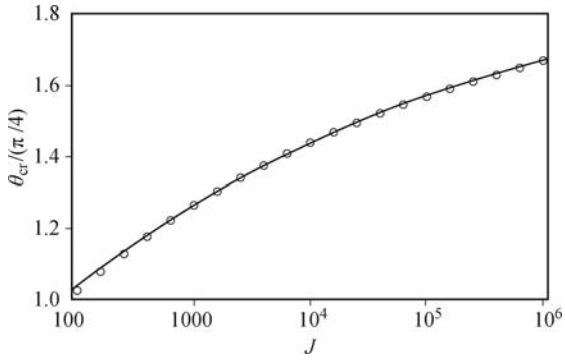

Fig. 3 Log–log plot of the critical polar angle $\theta_{\rm cr}$ (in units of $\pi/4$) against J ($= N/2$) for the $\hat{J}_x$ measurement. The exact numerical results (*empty circles*) predict $\theta_{\rm cr} \simeq (1.216, 1.383, 1.522) \times \pi/4$ for $J = (10^3, 10^4, 10^5)$, fitting in Eq. (21) (*solid line*).

Similarly, for the $\hat{J}_y$ measurement, from Eq. (17) we find that the best-sensitivity phase obeys the transcendental equation

$$\cos\theta \tan\alpha = 2J\phi \sin^2\theta \tag{22}$$

which gives $(\delta\phi_y)_{\rm min} \simeq 1/(\sqrt{2}J^{3/2}|\sin(2\theta)|)$. For the case $\theta = \pi/4$ or $3\pi/4$, Eq. (22) reduces to $\tan\alpha = \alpha$ with the solutions $\alpha = \sqrt{2}J\phi = 0, \pm 1.42\pi, \pm 2.46\pi$, *etc.*. As shown in Fig. 1(b), one can find that including $\phi = 0$, the phase shift $|\phi| < 0.2\pi/(\sqrt{2}J)$ can be detected at the super-Heisenberg limit for the $\hat{J}_y$ measurement (*empty circles*).

The scaling rules of the best sensitivity can be shown in a more transparent form by setting $(\delta\phi_v)_{\rm min} = \kappa J^{-\xi_v}$ (with $v = x, y$) [14], where κ denotes a prefactor and ξ_v the scaling exponent for $\hat{J}_v$ measurements. From Eq. (20), it is easy to obtain

$$\xi_v = -\frac{\ln[\sqrt{2}(\delta\phi_v)_{\rm min}]}{\ln J} \simeq \frac{3}{2} + \frac{\ln(|\sin(2\theta)|)}{\ln J} \tag{23}$$

where we take $\kappa = 1/\sqrt{2}$ to ensure $\xi_v \to 3/2$ as $\theta \to \pi/4$ or $3\pi/4$. In Fig. 2(b), numerical simulations of the scaling exponent is plotted as a function of θ. In the absence of the dephasing, one can find that ξ_x (*empty circles*) and ξ_y (*crosses*) agree very well with the analytical result of Eq. (23) (*dashed red line*). For $\theta_{\rm cr} < \theta < (\pi - \theta_{\rm cr})$, the numerical result of ξ_x deviates from the analytical one due to the bifurcation of the best-sensitivity phase $\phi_{\rm min}$. In fact, slightly different sensitivities can be obtained if we substitute Eq. (18) and Eq. (19) into Eq. (16).

4.2 With the dephasing

It is worthy pointing out that our analytical results, Eq. (16) and Eq. (17) break down when $\theta \simeq \pi/2$. In this case, $\cos\theta \simeq \alpha \simeq 0$ and hence Eq. (15) reduces to $\mathrm{d}\langle\hat{J}_+\rangle/\mathrm{d}\phi \simeq -2J^2\phi \mathrm{e}^{-\beta}$. Due to $\mathrm{d}\langle\hat{J}_y\rangle/\mathrm{d}\phi = 0$ and thus $\delta\phi_y \to \infty$, there is no signal from the $\hat{J}_y$ measurement. However, $\delta\phi_x$ can nevertheless reach the Heisenberg limit [13]. To see this clearly, we solve the approximated result of the sensitivity as

$$(\delta\phi_x)^2 \simeq \frac{1}{2J^2}\left[1 + (J\phi + \gamma)^2 + \frac{\gamma}{2J\phi}\right] \tag{24}$$

where we have expanded η_0 and η_1 of Eq. (13) up to the first- and the second-order of β. Without the dephasing (i.e., $\gamma = 0$), Eq. (24) reduces to $\delta\phi_x \simeq (1 + J^2\phi^2)^{1/2}/(\sqrt{2}J)$, which is minimized for $\phi = 0$, or more generally $\phi = s\pi$ with an integer s. It is interesting to note that though the slop of the signal $\mathrm{d}\langle\hat{J}_x\rangle/\mathrm{d}\phi \simeq -2J^2\phi$, proportional to N^2, the achievable phase sensitivity can reach only the Heisenberg limit $(\delta\phi_x)_{\rm min} \simeq 1/(\sqrt{2}J) = \sqrt{2}/N$ due to the enhanced variance $(\Delta\hat{J}_x)^2 \simeq \frac{J}{2}(4J\phi^2)$ [24].

In Fig. 4, we plot Eq. (24) as a function of ϕ for $\gamma = 0$ (*thin black*) and 10^2 (*thick red line*). Within the small-phase region, our analytical result displays a remarkable agreement with numerical simulations. For a relatively large dephasing ($\gamma \gg 1$), the achievable sensitivity $(\delta\phi_x)_{\rm min} \simeq \gamma/(\sqrt{2}J)$, corresponding to the scaling exponent $\xi_x \simeq 1 - \ln\gamma/\ln J \simeq 0.5$ for $J = 10^4$ and $\gamma = 10^2$ [see the triangle of Fig. 2(b) at $\theta = \pi/2$].

Finally, we investigate the achievable sensitivities for $\theta \neq \pi/2$ case. Due to a weak phase dephasing (with $\gamma = \Gamma/\chi = 1$), the CSS with $\theta = \pi/6$ or $5\pi/6$ becomes the optimal input state, which gives a better sensitivity for the $\hat{J}_x$ measurement [see solid red line of Fig. 1(c) at $\phi \sim 0.5\pi/(\sqrt{2}J)$]. For the $\hat{J}_y$ measurement, the optimal sensitivity still occurs at $\phi \sim 0$ with $\theta = \pi/4$ or $3\pi/4$ [see Fig. 1(d)].

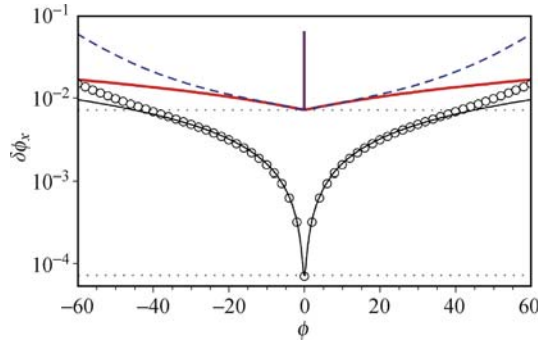

Fig. 4 Phase sensitivity $\delta\phi_x$ as a function of ϕ [in units of $\pi/(\sqrt{2}J)$] for $\theta = \pi/2$ and $J = N/2 = 10^4$. Thin solid line (*empty circles*) and thick red line (*dashed blue line*) are analytical (numerical) results of $\delta\phi_x$ for the dephasing rate $\gamma = 0$ and 10^2, respectively. Horizontal lines denote the Heisenberg limit of $1/(\sqrt{2}J)$ and $\gamma/(\sqrt{2}J)$.

With the increase of the dephasing rate, the CSS with $\theta = \pi/6$ or $5\pi/6$ is the optimal input state for both $\hat{J}_x$ and $\hat{J}_y$ measurements. To prove it, let us consider a relatively large dephasing rate ($1 \ll \gamma < J^{3/4}$). From

Fig. 1(e), we note that the best sensitivity occurs when $J\phi \ll 1$ and hence $\cot\alpha \sim \alpha^{-1} \gg 1$. As a result, Eq. (16) can be simplified as

$$(\delta\phi_x)^2 \simeq \frac{1}{2J^3\sin^2(2\theta)}\left[(4J\phi)^{-2} + 4\gamma J\phi\sin^2\theta\right] \quad (25)$$

where only the terms proportional to $\cot^2\alpha$ and γ are kept in the numerator of Eq. (16). Eq. (25) corresponds to the envelope curve of the sensitivity [38]. Minimizing it with respect to ϕ, we further obtain the best sensitivity $(\delta\phi_x)^2_{\min} \simeq 3\gamma^{2/3}/(8J^3\sin^{2/3}\theta\cos^2\theta)$ and the scaling exponent

$$\xi_x \simeq \frac{3}{2} + \frac{\ln\left[\frac{2}{\sqrt{3}}\gamma^{-1/3}\sin^{1/3}\theta|\cos\theta|\right]}{\ln J} \quad (26)$$

As shown in Fig. 2(b), our analytical result (*solid line*) shows a good agreement with numerical simulations (*triangles*) for $J = 10^4$ and $\gamma = 10^2$. Maximizing Eq. (26) with respect to θ, we get the optimal polar angle of the CSS $\theta = \pi/6$ or $5\pi/6$, which gives $(\delta\phi_x)_{\min} \simeq (2\gamma)^{1/3}/(\sqrt{2}J^{3/2})$ and the scaling exponent $\xi_x \simeq 3/2 - \ln(2\gamma)/(3\ln J)$ for the best-sensitivity phase $\phi_{\min} \simeq (2\gamma)^{-1/3}/J$ [see grid lines of Fig. 1(e) and Fig. 2(b)].

To find out the optimal sensitivity for the $\hat{J}_y$ measurement, we consider again the relatively large dephasing with $1 \ll \gamma < J^{3/4}$, for which Eq. (17) can be approximated as

$$(\delta\phi_y)^2 \simeq \frac{1}{2J^3\sin^2(2\theta)}\left(1 + 4\gamma J\phi\sin^2\theta\right) \quad (27)$$

where only the term proportional to γ ($\gg 1$) is kept due to $J\phi \ll 1$ and hence $\tan\alpha \sim \alpha \ll 1$. From Eq. (27), we obtain the phase sensitivity $\delta\phi_y \propto [1 + 2\gamma J\phi]^{1/2}$ and $[\frac{2}{\sqrt{3}}(1 + \gamma J\phi)]^{1/2}$ for the cases $\theta = \pi/4$ and $\pi/6$, respectively. Note that the slop of $\delta\phi_y$ for the case $\theta = \pi/6$ is smaller than that of $\theta = \pi/4$. In other words, except $\phi = 0$, a slightly better sensitivity can be obtained for the CSS with $\theta = \pi/6$ or $\theta = 5\pi/6$ [see solid red line of Fig. 1(f)].

5 Conclusions

In summary, we have investigated atomic Ramsey interferometer with the phase accumulation relying on free evolution of a coherent spin state $|\theta, 0\rangle$ under the Hamiltonian $\chi(\hat{J}_z)^k$. Compared with a linear interferometer (i.e., $k = 1$), the precision of the phase shift $\phi = \chi t$ for a nonlinear one (with $k = 2$) can be improved from the shot-noise limit $1/N^{1/2}$ to the super-Heinsenberg limit $2/N^{3/2}$, provided that an optimal CSS with $\theta = \pi/4$ or $3\pi/4$ is adopted as the input [14, 15]. According to the error propagation theory, the improved scaling is a consequence of the nonlinearity-induced phase accumulation [12], which yields the slop and the fluctuation of the Ramsey signal proportional to $(N/2)^2$ and $\sqrt{N}/2$, respectively.

Following a recent work [14], we analyze the role of collisional dephasing on the BEC-based nonlinear Ramsey interferometer. In the limit of small phase shift ϕ and large particle number N ($= 2J$), we derive analytical expressions of the phase sensitivities for spin operators $\hat{J}_x$ and $\hat{J}_y$ measurements after the phase accumulation. Our results, valid for $\theta \neq \pi/2$ and $\gamma < J^{3/4}$, show good agreement with numerical simulations. Without the collisional dephasing, we find that the best-sensitivity phase $\phi_{\min}$ satisfies different transcendental equations, depending upon the initial state and the observable being measured. For the $\hat{J}_x$ measurement, $\phi_{\min}$ bifurcate at the critical polar angle $\theta_{\rm cr} \simeq \arctan(0.6J^{1/8})$, as shown in Fig. 2(a) and Fig. 3; while for $\hat{J}_y$ measurement, the phase $|\phi| < 0.2\pi/(\sqrt{2}J)$ can be detected at super-Heisenberg limit. With the increase of the dephasing rate up to $J^{3/4}$, we find that the CSS with $\theta = \pi/6$ or $5\pi/6$ gives rise to a better sensitivity. Specifically, the phase shift $\phi_{\min} \simeq (2\gamma)^{-1/3}/J$ (~ 0) can be detected at the $N^{-3/2}$ scaling rule for the $\hat{J}_x$ ($\hat{J}_y$) measurement.

Additionally, we present analytical result of the sensitivity for the case $\theta = \pi/2$, which has been excluded in Ref. [38]. Our results show that although the slop of the signal increases as $\mathrm{d}\langle\hat{J}_x\rangle/\mathrm{d}\phi \propto N^2/2$, the variance is also enhanced $(\Delta\hat{J}_x) \propto N/\sqrt{2}$, leading to the phase sensitivity $\sqrt{2}/N$ in the end [13]. To improve phase resolution over the Heisenberg limit, it requires a super-resolution of the interferometric signal with its slop proportional to N^2 and also a reduced variance below the SNL. Both of them should be fulfilled simultaneously.

Acknowledgements This work was supported by the National Natural Science Foundation of China (Grant No. 10804007) and the Specialized Research Fund for the Doctoral Program of Higher Education (SRFDP) (Grant No. 200800041003). L. You was partially supported by the National Basic Research Program of China (Grant Nos. 2006CB921206 and 2006AA06Z104).

References

1. C. M. Caves, Phys. Rev. D, 1981, 23: 1693
2. B. Yurke, S. L. McCall, and J. R. Klauder, Phys. Rev. A, 1986, 33(6): 4033
3. M. J. Holland and K. Burnett, Phys. Rev. Lett., 1993, 71: 1355
4. T. Kim, O. Pfister, M. J. Holland, J. Noh, and J. L. Hall, Phys. Rev. A, 1998, 57: 4004
5. D. J. Wineland, J. J. Bollinger, W. M. Itano, and D. J. Heinzen, Phys. Rev. A, 1994, 50(1): 67
6. D. Leibfried, M. D. Barrett, T. Schaetz, J. Britton, J. Chiaverini, W. M. Itano, J. D. Jost, C. Langer, and D. J. Wineland, Science, 2004, 304: 1476
7. M. W. Mitchell, J. S. Lundeen, and A. M. Steinberg, Nature,

2004, 429: 161

8. V. Giovannetti, S. Lloyd, and L. Maccone, Science, 2004, 306: 1330
9. J. J. Bollinger, W. M. Itano, D. J. Wineland, and D. J. Heinzen, Phys. Rev. A, 1996, 54: R4649
10. R. A. Campos, C. C. Gerry, and A. Benmoussa, Phys. Rev. A, 2003, 68: 023810
11. P. M. Anisimov, G. M. Raterman, A. Chiruvelli, W. N. Plick, S. D. Huver, H. Lee, and J. P. Dowling, Phys. Rev. Lett., 2010, 104: 103602
12. A. Luis, Phys. Lett. A, 2004, 329: 8
13. A. M. Rey, L. Jiang, and M. D. Lukin, Phys. Rev. A, 2007, 76: 053617
14. S. Boixo, A. Datta, S. T. Flammia, A. Shaji, E. Bagan, and C. M. Caves, Phys. Rev. A, 2008, 77: 012317
15. S. Choi and B. Sundaram, Phys. Rev. A, 2008, 77: 053613
16. M. J. Woolley, G. J. Milburn, and C. M. Caves, New J. Phys., 2008, 10: 125018
17. A. Sørensen, L.-M. Duan, J. I. Cirac, and P. Zoller, Nature, 2001, 409: 63
18. T. Schumm, S. Hofferberth, L. M. Andersson, S. Wildermuth, S. Groth, I. Bar-Joseph, J. Schmiedmayer, and P. Krüger, Nature Phys., 2005, 1: 57
19. Y. Shin, C. Sanner, G.-B. Jo, T. A. Pasquini, M. Saba, W. Ketterle, and D. E. Pritchard, Phys. Rev. A, 2005, 72: 021604(R)
20. L. Pezzé, A. Smerzi, G. P. Berman, A. R. Bishop, and L. A. Collins, Phys. Rev. A, 2006, 74: 033610
21. A. D. Cronin, J. Schmiedmayer, and D. E. Pritchard, Rev. Mod. Phys., 2009, 81: 1051
22. C. Gross, T. Zibold, E. Nicklas, J. Estève, and M. K. Oberthaler, Nature, 2010, 464: 1165
23. M. F. Riedel, P. Böhi, Y. Li, T. W. Hänsch, A. Sinatra, and P. Treutlein, Nature, 2010, 464: 1170
24. M. Kitagawa and M. Ueda, Phys. Rev. A, 1993, 47(6): 5138
25. A. Imamoḡlu, M. Lewenstein, and L. You, Phys. Rev. Lett., 1997, 78: 2511
26. G. R. Jin, Y. C. Liu, and W. M. Liu, New J. Phys., 2009, 11: 073049
27. G. R. Jin, B. B. Wang, and Y. W. Lu, Chin. Phys. B, 2010, 19: 020502
28. D. Mahler, P. Joanis, R. Vilim, and H. de Guise, New J. Phys., 2010, 12: 033037
29. K. Mølmer and A. Sørensen, Phys. Rev. Lett., 1999, 82: 1835
30. L. You, Phys. Rev. Lett., 2003, 90: 030402
31. M. Zhang and L. You, Phys. Rev. Lett., 2003, 91: 230404
32. A. M. Rey, L. Jiang, M. Fleischhauer, E. Demler, and M. D. Lukin, Phys. Rev. A, 2008, 77: 052305
33. A. Widera, O. Mandel, M. Greiner, S. Kreim, T. W. Hänsch, and I. Bloch, Phys. Rev. Lett., 2004, 92: 160406
34. A. Widera, S. Trotzky, P. Cheinet, S. Fölling, F. Gerbier, I. Bloch, V. Gritsev, M. D. Lukin, and E. Demler, Phys. Rev. Lett., 2008, 100: 140401
35. D. Walls and G. Milburn, Quantum Optics, Berlin: Spinger-Verlag, 1994: 210
36. S. F. Huelga, C. Macchiavello, T. Pellizzari, A. K. Ekert, M. B. Plenio, and J. I. Cirac, Phys. Rev. Lett., 1997, 79: 3865
37. D. Ulam-Orgikh and M. Kitagawa, Phys. Rev. A, 2001, 64: 052106
38. Y. C. Liu, G. R. Jin, and L. You, Phys. Rev. A, 2010, 82: 045601
39. J. M. Radcliffe, J. Phys. A, 1971, 4: 313
40. F. T. Arecchi, E. Courtens, R. Gilmore, and H. Thomas, Phys. Rev. A, 1972, 6: 2211
41. S. Raghavan, H. Pu, P. Meystre, and N. P. Bigelow, Opt. Commun., 2001, 188: 149
42. R. R. Puri and G. S. Agarwal, Phys. Rev. A, 1992, 45: 5073
43. T. W. Chen and P. T. Leung, Phys. Rev. A, 2003, 67: 055802
44. Y. Khodorkovsky, G. Kurizki, and A. Vardi, Phys. Rev. A, 2009, 80: 023609
45. M. G. Genoni, S. Olivares, and M. G. A. Paris, arXiv: 1012.1123v4, 2011